Complex trajectory method in time-dependent WKB

Yair Goldfarb[1], Jeremy Schiff[1,2,3] and David J. Tannor[1]

[1]*Department of Chemical Physics,*

[2]*Department of Mathematics,*

The Weizmann Institute of Science,

Rehovot, 76100 Israel

March 6, 2008

Abstract

We present a significant improvement to a complex time-dependent WKB (CWKB) formulation developed by Boiron and Lombardi [JCP **108**, 3431 (1998)] in which the time-dependent WKB equations are solved along classical trajectories that propagate in complex space. Boiron and Lombardi showed that the method gives very good agreement with the exact quantum mechanical result as long as the wavefunction does not exhibit interference effects such as oscillations and nodes. In this paper we show that this limitation can be overcome by superposing the contributions of *crossing* trajectories. Secondly, we demonstrate that the approximation improves when incorporating higher order terms in the expansion. Thirdly, equations of motion for caustics and Stokes lines are implemented to help overcome Stokes discontinuities. These improvements could make the CWKB formulation a competitive alternative to current time-dependent semiclassical methods.

[3]On sabbatical leave from Dept. of Mathematics, Bar-Ilan University, Ramat Gan 52900, Israel.

PACS numbers:

I. INTRODUCTION

The difficulty in performing quantum mechanical calculations of multi-dimensional systems has stimulated an intensive and ongoing effort in the last four decades to develop numerical tools based on semiclassical mechanics. In this context, we refer to semiclassical mechanics as the calculation of a quantum mechanical wavefunction or propagator via propagation of classical (or classical-like) trajectories. From a physical point of view, semiclassical methods try to evade the non-locality imbedded in quantum mechanics. Mathematically speaking, semiclassical methods aim at casting the time-dependent Schrödinger equation (TDSE), which is a PDE, in terms of ODEs related to classical equations of motion. This transformation has significant computational advantages that can ease the inherent difficulty of multi-dimensional quantum calculations.

The WKB method[1] can be considered as the first of the semiclassical methods. Its date of birth almost coincides with the publication of the Schrödinger equation in 1926, and virtually every standard text book in quantum mechanics has a description of the method. The basic idea of the WKB method is to recast the wavefunction as the exponential of a function and expand the function as a power series in $\hbar$. The WKB method is ordinarily applied to the *time-independent* Schrödinger equation and provides for a good approximation to the eigenstates as long as one is not too near a classical turning point. It is only natural that as part of the effort to develop time-dependent semiclassical methods, a time-dependent version of the WKB method would be explored. Surprisingly little work has been done in this direction[2–14]. A decade ago, Boiron and Lombardi[15] developed a complex trajectory version of time-dependent WKB, which we refer to as CWKB. In conventional WKB the leading order term in the phase of the wave function is taken to be $O(\hbar^{-1})$ and the leading order term in the amplitude is taken to be $O(\hbar^{0})$. In contrast, the CWKB formulation treats the amplitude and phase on an equal footing by using a complex phase which is expanded in powers of $\hbar$. The leading order term in both the amplitude and phase is $O(\hbar^{-1})$. The price to pay for this procedure is that the resulting classical trajectories propagate in complex space.

The CWKB equations of motion can be solved analytically and yield the *exact* wavefunction for an initial Gaussian wavepacket in a potential with up to quadratic terms. The first-order method was tested numerically by Boiron and Lombardi for scattering of a Gaus-

sian wavepacket from a potential barrier. They showed that the method produced very good results as long as the wavefunction did not exhibit *interference effects* in the form of oscillations or nodes[15]. In this paper we present a simple modification to CWKB that provides an accurate description of oscillations in the wavefunction. We show that complex classical trajectories, similar to real classical trajectories, can cross in configuration space. By superposing the contributions from two or more crossing trajectories, interference effects are obtained. We also show that the CWKB approximation generally improves when incorporating additional terms in the series expansion. Since the WKB expansion is an asymptotic series, this observation is non-trivial. The use of complex trajectories introduces caustics and Stokes discontinuities[28, 36, 42]. In this paper we apply equations of motion for the caustic and the Stokes lines to partly overcome the difficulties arising from these two phenomena.

Three other semiclassical formulations that incorporate complex trajectories should be mentioned in relation with CWKB. The first is the Generalized Gaussian Wavepacket Dynamics (GGWPD) developed by Huber, Heller and Littlejohn [16, 17]. One may show that for an initial Gaussian wavepacket the equations of motion of GGWPD are de facto identical to the equations of the first-order approximation of CWKB. However the GGWPD has no generalization to arbitrary initial wavefunctions and no systematic way to increase the accuracy of the approximation. On the other hand, Huber and Heller[16] appreciate the importance of multiple complex trajectories in obtaining interference phenomena. Here we incorporate the idea of crossing complex trajectories into the more general CWKB formulation.

Strongly related to the work of Huber and Heller, but developed from a completely different angle, is the extensive work by de Aguiar and collaborators on semiclassical approximations to the coherent state propagator, both in one[18–22] and multiple[23–25] dimensions (This work extends earlier work on the coherent state propagator by Klauder[26], Weissman [27], Adachi[28] and Rubin and Klauder[29]). Once again, this work is restricted to specific initial and final wavefunctions, but the formalism does in principle allow calculations of increasing accuracy, and a detailed study of the need for multiple trajectories has been undertaken[20].

The final formulation that is closely related is Bohmian Mechanics with Complex Action (BOMCA)[30–35]. CWKB and BOMCA begin with the same ansatz, substituting $\psi =$

$\exp(iS/\hbar)$ into the TDSE. Like CWKB, the BOMCA formulation uses equations of motion that propagate along complex trajectories, and in fact the first-order equations of motion of BOMCA are identical to the equations of first-order CWKB. The differences between the two formulations are: (1) In CWKB the equations of motion are for the coefficients of an $\hbar$ Taylor series expansion of the phase and their spatial derivatives. The equations of motion in BOMCA are for the coefficients of the spatial derivatives of the phase, without any $\hbar$ expansion. (2) Incorporating higher order terms of the CWKB approximation does not affect the results for lower order terms: each equation of motion depends only on lower terms of the expansion. This is not the case with BOMCA where each equation of motion depends on both lower and higher terms, giving rise to feedback. (3) A consequence of (2) is that in CWKB the equations of motion of the trajectories remain *classical* whereas in BOMCA, the inclusion of higher orders of approximation affect the complex trajectories by adding a "quantum force" that yields *quantum* trajectories.

The CWKB method suffers from two drawbacks that limit semiclassical methods in general. The first of these is the appearance of *caustics*[36]. The caustics are familiar from the semiclassical literature as the positions where the van Vleck determinant diverges[37], hence, in the vicinity of a caustic semiclassical approximations yield inaccurate results. In CWKB (as in GGWPD or BOMCA) the caustics propagate in the complex plane and as they cross the real axis their deleterious effect is most evident. The caustics are also the positions from where *Stokes lines* originate[28]. Stokes lines define the boundaries between regions where the number of contributing solutions to the wavefunction changes[38]. Although Stokes lines can be determined a posteriori, a general formulation that predicts the position of caustics and Stokes lines and overcomes the difficulties they present is still an active field of research[17, 22, 25, 28, 39–41]. Currently, discarding non-physical solutions remains the most general and easily applied criterion[21, 23]. A significant step in overcoming the difficulty presented by the Stokes phenomenon and the discarding of non-physical solutions was derived by Berry[42] who obtained a "smoothing" function in the vicinity of where a Stokes line crosses the real axis. This function phases out the non-physical solutions in a smooth way which prevents the discontinuity that appears when a non-physical solutions is suddenly discarded. In this paper we present a significant improvement to current methodologies by writing *equations of motion of the Stokes lines* (and the caustics). These equations allow us to trace numerically the position where the Stokes line crosses the real

axis as a function of time. Combining this result with Berry's smoothing function is a novel way of dealing with the difficulties posed by the Stokes phenomena.

This paper is organized as follows. In Section II we formulate the CWKB method. Our derivation is more compact than the Boiron-Lombardi derivation, providing the equations of motion for higher orders of the expansion in a simple manner. In this Section (II D) we also discuss the issues raised by caustics and Stokes lines. In Section III we apply the formulation to a Gaussian initial wavepacket propagating in a quartic double-well potential. We demonstrate that superposing the contributions of crossing trajectories leads to interference effects and that incorporating higher order terms in the expansion improves the approximation. Section IV contains a summary and concluding remarks.

II. FORMULATION

A. Time-independent vs. Time-dependent WKB

For simplicity we present the one-dimensional version of the CWKB derivation. The generalization to multi-dimensions can be performed in a straightforward manner[44]. The conventional WKB derivation begins by inserting the ansatz

$$\psi(x) = \exp\left(\frac{i}{\hbar}S(x)\right), \tag{2.1}$$

into the *time-independent* Schrödinger equation, where $\hbar$ is Planck's constant divided by 2π. The result is

$$\frac{1}{2m}\left(\frac{dS}{dx}\right)^2 + V(x) - \frac{i\hbar}{2m}\frac{d^2S}{dx^2} = E, \tag{2.2}$$

where m is the mass of the particle, $V(x)$ is the potential energy and E is the energy eigenvalue. If we assume that $S(x)$ can be expanded asymptotically as a power series in $\frac{\hbar}{i}$

$$S(x) = S_0(x) + \frac{\hbar}{i}S_1(x) + \left(\frac{\hbar}{i}\right)^2 S_2(x) + ... = \sum_{j=0}^{\infty}\left(\frac{\hbar}{i}\right)^j S_j(x), \tag{2.3}$$

then, by substituting the last equation into eq.(2.2) and equating powers of $\frac{\hbar}{i}$, a series of coupled real ODEs are obtained for the S_j's.

Time-dependent WKB begins by inserting the ansatz[2, 3]

$$\psi(x,t) = \exp\left(\frac{i}{\hbar}S(x,t)\right), \tag{2.4}$$

into the time-dependent Schrödinger equation,

$$i\hbar\partial_t\psi = -\frac{\hbar^2}{2m}\partial_{xx}\psi + V(x,t)\psi. \tag{2.5}$$

The result is the quantum Hamilton-Jacobi equation[2, 3]

$$\partial_t S + \frac{1}{2m}(\partial_x S)^2 + V = \frac{i\hbar}{2m}\partial_{xx}S, \tag{2.6}$$

where the LHS of the equation is in the form of the classical Hamilton-Jacobi equation. Equation (2.6) is formally exact. In the time-dependent WKB formulation one inserts into eq.(2.6) a time-dependent version of eq.(2.3)

$$S(x,t) = \sum_{j=0}^{\infty}\left(\frac{\hbar}{i}\right)^j S_j(x,t). \tag{2.7}$$

The result is

$$\sum_{j=0}^{\infty}\left(\frac{\hbar}{i}\right)^j \partial_t S_j + \frac{1}{2m}\sum_{j_1,j_2=0}^{\infty}\left(\frac{\hbar}{i}\right)^{j_1+j_2}\partial_x S_{j_1}\partial_x S_{j_2} + V = -\frac{1}{2m}\sum_{j=0}^{\infty}\left(\frac{\hbar}{i}\right)^{j+1}\partial_{xx}S_j. \tag{2.8}$$

By equating terms having the same powers of $\frac{\hbar}{i}$ we obtain the classical Hamilton-Jacobi equation for $S_0(x,t)$

$$\partial_t S_0 + \frac{1}{2m}(\partial_x S_0)^2 + V = 0, \tag{2.9}$$

and equations of motion for $S_n(x,t), n \geq 1$

$$\partial_t S_n + \frac{\partial_x S_0}{m}\partial_x S_n = -\frac{1}{2m}\partial_{xx}S_{n-1} - \frac{1}{2m}\sum_{j=1}^{n-1}\partial_x S_j \cdot \partial_x S_{n-j}. \tag{2.10}$$

We note that the RHS of the equation of motion for S_n depends only on $S_1, ..., S_{n-1}$ and their derivatives, i.e. terms of orders lower than n. The next step in time-dependent WKB is to convert eqs.(2.9) and (2.10) into a set of ODEs by calculating the evolution of $S_0, S_1, \ldots$ along classical trajectories, as described in the next section.

B. Integrating along classical trajectories

As mentioned earlier, the first term in the $\hbar$ power expansion, S_0, obeys the classical Hamilton-Jacobi equation (eq.(2.9)). This equation, which is a PDE for the action field S, can be transformed into Newton's second law of motion by going into a moving frame,

i.e. by using the Lagrangian time derivative. This suggests solving not only eq.(2.9) but also eq.(2.10) by using the Lagrangian time derivative, i.e. by integrating along classical trajectories.

The link between the Hamilton-Jacobi equation and classical trajectories is established by defining the *velocity field*

$$v(x,t) \equiv \frac{\partial_x S_0(x,t)}{m} \tag{2.11}$$

and considering the trajectories defined by

$$\frac{dx}{dt} = v(x,t) \ . \tag{2.12}$$

By taking the spatial partial derivative of eq.(2.9), using the definition of the Lagrangian time derivative $\frac{d}{dt} \equiv \partial_t + \frac{dx}{dt}\partial_x$, and applying eq.(2.11) we obtain the equation of motion for the velocity along a trajectory as Newton's second law

$$\frac{dv}{dt} = -\frac{\partial_x V}{m}. \tag{2.13}$$

Hence, the trajectories defined are simply classical trajectories.

By the same token, we may calculate the Lagrangian time derivative of the action field. Using eq.(2.9) we find S_0 satisfies

$$\frac{dS_0}{dt} = \partial_t S_0 + \frac{\partial S_0}{m}\partial_x S_0 = \frac{1}{2}mv^2 - V. \tag{2.14}$$

We recognize this as the equation of motion for the action along a classical trajectory. Noting that v is just an auxiliary variable, the equations of motion for the zeroth-order term of time-dependent WKB, S_0, can be summarized as

$$\frac{dx}{dt} = \frac{\partial_x S_0}{m}, \tag{2.15}$$

$$\frac{d(\partial_x S_0)}{dt} = -\partial_x V, \tag{2.16}$$

$$\frac{dS_0}{dt} = \frac{1}{2m}(\partial_x S_0)^2 - V. \tag{2.17}$$

We turn to the higher order terms in the series S_n, $n \geq 1$. Recognizing the LHS of eqs.(2.10) as the Lagrangian time derivative of S_n, we can write

$$\frac{dS_n}{dt} = -\frac{1}{2m}\partial_{xx} S_{n-1} - \frac{1}{2m}\sum_{j=1}^{n-1} \partial_x S_j \cdot \partial_x S_{n-j}. \tag{2.18}$$

These equations do not constitute a closed set of ODEs since they depend on partial derivatives such as $\partial_{xx}S_{n-1}$. We close the set of equations by deriving equations of motion for the partial derivatives on the RHS of eq.(2.18) ($\partial_{xx}S_{n-1}$ and $\partial_x S_j, j = 1, ..., (n-1)$). Consider for example the equations of motion for S_1 and S_2. Inserting $n = 1$ in eq.(2.18) yields

$$\frac{dS_1}{dt} = -\frac{1}{2m}\partial_{xx}S_0. \tag{2.19}$$

An equation of motion for $\partial_{xx}S_0$ is obtained by taking a second spatial partial derivative of eq.(2.9),

$$\partial_{xxt}S_0 + \frac{1}{m}\left(\partial_x S_0 \cdot \partial_{xxx}S_0 + (\partial_{xx}S_0)^2\right) + \partial_{xx}V = 0, \tag{2.20}$$

and rewriting it as

$$\frac{d(\partial_{xx}S_0)}{dt} = -\frac{1}{m}(\partial_{xx}S_0)^2 - \partial_{xx}V. \tag{2.21}$$

Equations (2.19) and (2.21) provide a closed set of equations of motion for S_1. Equation (2.21) is derived in reference [15] by a cumbersome finite difference scheme. It is equivalent to eq.(2.9d) of reference [17] where the equation appears in the context of GGWPD. An equation of motion for any order of spatial derivative of S_0 can be derived in a similar fashion by taking consecutive spatial derivatives of eq.(2.20) and then grouping together the Lagrangian time derivative terms.

Inserting $n = 2$ into eq.(2.18) yields

$$\frac{dS_2}{dt} = -\frac{1}{2m}\partial_{xx}S_1 - \frac{1}{2m}(\partial_x S_1)^2. \tag{2.22}$$

The equations of motion for $\partial_x S_1$ and $\partial_{xx}S_1$ are obtained by first inserting $n = 1$ into eq.(2.10). We then derive two equations by taking a first and a second spatial partial derivative of the result. By grouping the Lagrangian time derivatives of $\partial_x S_1$ and $\partial_{xx}S_1$ in each of the two equations separately we obtain

$$\frac{d(\partial_x S_1)}{dt} = -\frac{1}{2m}\partial_{xxx}S_0 - \frac{1}{m}\partial_x S_1 \cdot \partial_{xx}S_0, \tag{2.23}$$

$$\frac{d(\partial_{xx}S_1)}{dt} = -\frac{1}{2m}\partial_{xxxx}S_0 - \frac{1}{m}\partial_x S_1 \cdot \partial_{xxx}S_0 - \frac{2}{m}\partial_{xx}S_1 \cdot \partial_{xx}S_0. \tag{2.24}$$

The last equations depend in turn on $\partial_{xxx}S_0$ and $\partial_{xxxx}S_0$. As mentioned earlier, the equation of motion for these terms can be obtained by additional spatial derivatives of eq.(2.20), a process that yields

$$\frac{d(\partial_{xxx}S_0)}{dt} = -\frac{3}{m}\partial_{xx}S_0 \cdot \partial_{xxx}S_0 - \partial_{xxx}V, \tag{2.25}$$

$$\frac{d(\partial_{xxxx}S_0)}{dt} = -\frac{1}{m}\left(4\partial_{xx}S_0 \cdot \partial_{xxxx}S_0 - 3(\partial_{xxx}S_0)^2\right) - \partial_{xxxx}V. \tag{2.26}$$

Equations (2.22)-(2.26) provide a closed set of equations of motion needed for S_2. The scheme we have just described for S_1 and S_2 can be extended to any of the higher order terms in the expansion. Note that incorporating higher order terms S_n in the time-dependent WKB approximation does not affect the classical trajectories associated with S_0, defined by eqs.(2.15) and (2.16).

We now consider the number of equations as a function of N (the order of $\hbar$ retained in eq.(2.7)), and the dimensionality d. As seen above, for $d = 1$ and $\hbar$ truncation at orders 0,1 and 2 we require 3, 5 and 10 equations respectively. In general for $d = 1$, for truncation at order $N \geq 1$, $N^2 + 2N + 2$ equations are needed. For fixed truncation order $N \geq 1$, the number of equations scales polynomially with dimensionality as d^{2N} (for $N = 0$ there are $2d + 1$ equations, and for $N = 1$ there are $\frac{1}{2}(d + 1)(d + 4)$ equations). Thus, if one is interested in $\psi(x, t)$ at a specific point x at time t, there is potential here to evade the usual exponential growth of the work necessary to solve the Schrödinger equation as the dimension increases.

We now turn to the distinction between conventional time-dependent WKB and CWKB.

C. Initial conditions and complex classical trajectories

In conventional time-dependent WKB the initial wavefunction is "divided" between $S_0(x, 0)$ and $S_1(x, 0)$ by writing

$$\psi(x, 0) = A(x) \exp(i\phi(x)) = \exp\left(\frac{i}{\hbar}\left(S_0(x, 0) + \frac{\hbar}{i} S_1(x, 0)\right)\right), \tag{2.27}$$

where $A(x)$ and $\phi(x)$, the initial amplitude and phase respectively, are both taken to be real. The phase is related to the zero-order term S_0 and the amplitude to the first-order correction term S_1 according to

$$S_0(x, 0) = \hbar\phi(x), \quad S_1(x, 0) = \ln(A(x)), \tag{2.28}$$

and $S_n(x, 0) = 0$ for $n \geq 2$. Note that the initial conditions specified by eqs.(2.28) yield classical trajectories that propagate on the *real* axis since S_0 and its spatial derivatives are real quantities (see eqs.(2.15) and (2.16)).

In contrast, in CWKB the amplitude and phase are treated on an equal footing with far-reaching consequences. The initial wavefunction is related to $S_0(x, 0)$ by

$$S_0(x, 0) = -i\hbar \ln(\psi(x, 0)), \tag{2.29}$$

and $S_n(x,0) = 0$ for $n \geq 1$. Since S_0 is generally complex and since the initial velocity is $v(x,0) \equiv \partial_x S_0(x,0)/m$, the trajectories propagate in the *complex space* even if the initial positions are on the real axis ($\Im(x(0)) = 0$). This observation requires us to look at the analytic continuation of the wavefunction in complex space and find ways to extract the wavefunction on the real axis.

D. Complex root search and superposition

One of the differences between CWKB (as well as conventional time-dependent WKB) compared with BOMCA, is that the trajectories obey the classical equations of motion independent of the order of truncation in $\hbar$ in the final wavefunction. But, like BOMCA, for an arbitrary initial position $x(0) \in \mathbb{C}$ and an arbitrary final propagation time t_f, the final position $x(t_f)$ in CWKB is complex and yields an "analytically continued" wavefunction at $x(t_f)$

$$\psi(x(t_f), t_f) \approx \exp\left(\frac{i}{\hbar}\sum_{j=0}^{N}\left(\frac{\hbar}{i}\right)^j S_j(x(t_f), t_f)\right), \tag{2.30}$$

where N is the order of the truncation. References [15, 17, 30] discuss root search algorithms to find initial positions that reach the *real* axis at a given time. The central idea is to use the fact that the mapping $x(0) \mapsto x(t_f)$ is analytic, allowing for an iterative determination of the complex initial positions that lead to real final positions. However, as discussed in references [16, 17] and in section III A, for an arbitrary potential and final time, the mapping may not be one-to-one. Generally, more than one complex initial position ends at a given real (or complex) final position. This complicates the search for trajectories that end on the real axis but, as we shell see, allows for the possibility of interference effects.

A key point in this article is that the contribution of multiple trajectories in CWKB can accumulate to an interference pattern. Suppose that L trajectories end at final time t_f at the real position $x(t_f)$. Then one can make the ansatz that the final wavefunction can be approximated by a superposition of contributions

$$\psi(x(t_f), t_f) \approx \sum_{l=1}^{L} \exp\left(\frac{i}{\hbar} S^l\left(x(t_f), t_f\right)\right), \tag{2.31}$$

where each trajectory (denoted by the index l) is associated with a phase $S^l(x(t_f), t_f)$

$$S^l(x(t_f), t_f) = \sum_{j=0}^{N} \left(\frac{\hbar}{i}\right)^j S_j^l(x(t_f), t_f), \tag{2.32}$$

that is calculated by the CWKB equations of motion. As we discuss in the next section, the appearance of caustics and the Stokes phenomenon leads to a more complicated picture than that suggested by eq.(2.32).

E. Caustics and the Stokes phenomena

Although eqs. (2.31-2.32) are generally quite accurate, this ansatz breaks down at certain times and positions corresponding to caustics in the complex plane. Moreover, different regions in coordinate space may require different contributions (out of the L possibilities) to be incorporated into eq.(2.31). The boundaries between the different regions, which in general depend on time, are known as Stokes lines[38]. Reference [28] provides a scheme to find the Stokes lines, but in general this is a numerically cumbersome procedure. Moreover, the identification of the Stokes lines is a posteriori, meaning that the existence of the Stokes lines is not inferred until after a particular contribution of a complex trajectory is deemed to be non-physical.

In this paper we use equations of motion for the caustics and the Stokes lines to partly overcome the difficulties presented by these two phenomena. The position of the caustic is familiar from the semiclassical literature as the position where the van Vleck determinant diverges. Since it is possible to show the equivalence between S_1 and the van Vleck determinant[44], the caustic is traced by following the divergence of S_1. In appendix A we present the equations of motion of the caustic. Note that these equations do not predict where a caustic will appear but only yield the dynamics of a caustic. Knowing the position of a caustic allows us to predict when and where a caustic will approach the real axis, resulting in a local breakdown of our semiclassical approximation.

A schematic derivation of the equations of motion of the Stokes lines appear in appendix B. These equations allow us to trace the position where a Stokes line crosses the real axis. At the crossing point X_C, the number of contributing solutions may change as a non-physical solution is omitted. For the example in section III there are two contributions to the wavefunction, one of which becomes non-physical starting from the crossing position. Instead

of simply omitting this solution (resulting in a discontinuity) we use a smoothing function developed by Berry[42] and applied by van Voorhis and Heller[43]. Berry showed that in the vicinity of the crossing position a smooth transition of the Stokes lines is obtained by multiplying the dominant contribution (the contribution that diverges beyond the crossing point) by what he refers to as the *Stokes multiplier function*

$$G(x,t)=\begin{cases}1 & x\lesssim X_C\\ \frac{1}{2}\left(1-\mathrm{erf}\left(\frac{\Re(S_0^1-S_0^2)}{\sqrt{2\Im(S_0^1-S_0^2)}}\right)\right) & x\approx X_C\\ 0 & x\gtrsim X_C\end{cases}, \tag{2.33}$$

where $S_0^1=S_0^1(x,t)$ and $S_0^2=S_0^2(x,t)$ are the classical actions corresponding to the two contributions (S_0^2 corresponds to the contribution to be discarded). Note that x in eq.(2.33) is real and that $G(x,t)$ varies from zero to one. Hence, we rewrite eq.(2.31) for the case where there are two contributions

$$\psi(x,t)\approx\exp\left(\frac{i}{\hbar}S^1\left(x,t\right)\right)+G(x,t)\exp\left(\frac{i}{\hbar}S^2\left(x,t\right)\right), \tag{2.34}$$

where $t=t_f$ and $x=x(t_f)$. Far from the crossing point, $G(x,t)$ is taken to be either zero (in the direction of the classically forbidden zone) or one (in the classically allowed direction). Since eq.(2.33) is applicable only in the vicinity of the crossing point, its application in a time-dependent way requires knowing the dynamics of the crossing point. This is where the equation of motion of the Stokes line plays a role. In appendix B we present a schematic for the derivation of these equations. Here we suffice with writing the equation of motion for the crossing point X_C that can be extracted from these equations

$$\frac{dX_C}{dt}=\frac{\frac{1}{2}\Re(v_1^2-v_2^2)}{\Re(v_1-v_2)}, \tag{2.35}$$

where $v_1=\frac{1}{m}\frac{d}{dt}(\partial_x S_0^1)$ and $v_2=\frac{1}{m}\frac{d}{dt}(\partial_x S_0^2)$ are the velocities of the two trajectories at t_f at position X_C. In appendix B we also specify the equations of motion for the initial positions that reach X_C; these equations are needed for obtaining the v_j's. Given X_C at a given time we can use eq.(2.35) and the equations of motion for the initial positions to propagate X_C. Applying Berry's smoothing function at the time-dependent X_C allows us to pass over the Stokes lines in a continuous way.

III. NUMERICAL RESULTS

In this section we examine numerically the CWKB formulation allowing for the superposition of complex trajectories. For ready comparison with the work of Boiron and Lombardi the physical system we choose is identical to theirs (reference [15], Section IVB). The potential considered is a quartic double-well

$$V(x) = 1.25 \times 10^{-4}(x^4 - 400x^2), \tag{3.1}$$

with the initial wavefunction given by a Gaussian wavepacket

$$\psi(x,0) = \exp\left(-\alpha_0(x-x_c)^2 + \frac{i}{\hbar}p_c(x-x_c) + \frac{i}{\hbar}\gamma_0\right). \tag{3.2}$$

We take $\alpha_0 = 1$, $x_c = 0$, $p_c = 5$, $\gamma_0 = -\frac{i\hbar}{4}\ln(\frac{2\alpha_0}{\pi})$ and we set $m = \hbar = 1$ (all quantities are given in atomic units). The initial conditions for the terms in the $\hbar$ power-expansion of the phase are (see eq.(2.7) with eq.(2.29))

$$\begin{aligned}
S_0(x,0) &= i\alpha_0\hbar(x-x_c)^2 + p_c(x-x_c) + \gamma_0 = ix^2 + 5x + \gamma_0, && (3.3)\\
\partial_x S_0(x,0) &= 2i\alpha_0\hbar(x-x_c) + p_c = 2ix + 5, && (3.4)\\
\partial_{xx} S_0(x,0) &= 2i\alpha_0\hbar = 2i, && (3.5)\\
\partial_x^j S_0(x,0) &= 0,\ j \geq 3, && (3.6)\\
\partial_x^j S_k(x,0) &= 0,\ j \geq 0,\ k \geq 1, && (3.7)
\end{aligned}$$

where $\partial_x^j S_k \equiv \frac{\partial^j S_k}{\partial x^j}$.

In section III A we analyze the first order approximation of CWKB ($N = 1,\ S = S_0 + \frac{\hbar}{i}S_1$) and the properties of the trajectories. Section III B is dedicated to the next order of the approximation ($N = 2,\ S = S_0 + \frac{\hbar}{i}S_1 + \left(\frac{\hbar}{i}\right)^2 S_2$). We omit an analysis of $N = 0$ since it is well presented in reference [15] and yields poor results.

A. First Order approximation, $N = 1$

The first order approximation of CWKB requires the solution of eqs.(2.15), (2.16), (2.17), (2.19) and (2.21). The first two equations define the complex classical trajectories and the next three equations yield S_0 and S_1. We start by analyzing the complex classical trajectories. As mentioned above, the mapping $x(0) \mapsto x(t_f)$ is not one-to-one. For the

quartic potential, we found at least three initial positions that are mapped to every real final position at $t_f > 0$. For short time scales this observation can be supported analytically. For general potentials or for longer time scales than we present here, more than three initial positions might be relevant[17, 46]. In figures 1(a) and 1(b) we plot complex classical trajectories for $t_f = 3$ and $t_f = 6$ respectively. The *initial* positions of the trajectories can be divided into three sets referred to in ref.[17] as *branches*. Following ref.[16], one set is called the 'real branch' and the other sets are called the 'secondary branches'. The real branch is characterized by the property that it includes the initial position of a trajectory that propagates *solely* on the real axis, which we refer to as the real trajectory. It can be readily verified that for a Gaussian initial wavefunction there is only a single real trajectory, beginning at $x(0) = x_c$ (see eqs.(2.15), (2.16) and (3.4)). In fig.1(b) we depict the real trajectory explicitly. The secondary branches are defined as the loci of initial positions that do not belong to the real branch. Generally, the branches are infinitely long curves in the complex plane although only along a finite portion do they correspond to final positions where the wavefunction is significantly different from zero. In our figures below the branches are depicted as curves of *finite* length in the complex plane, although clearly there is some arbitrariness to their length.

In fig.1(a) we see that the real branch is centered in the vicinity of the real axis at all times. The initial position $x(0) = x_c$ is guaranteed to be located in the real branch and this prevents the real branch (recall that this is the locus of *initial* positions) from "straying" from the neighborhood of the real axis as the final time t_f is increased. At short time scales, the secondary branches are centered far from neighborhood of the real axis. Note that the linear dependence of the initial momentum on position (eq.(3.4)) allows trajectories with initial positions far from the real axis to reach a real final position in a short time. We can show analytically that for small times t_f the initial positions that comprise the real branch obey $|x(0)| = O(t_f)$ whereas the secondary branches obey $|x(0)| = O(\frac{1}{t_f})$. At intermediate times (times comparable to the time of the collision of the wavefunction with the barrier, $4 \lesssim t_f \lesssim 7$), secondary branch (1) reaches the vicinity of the real axis (cf. fig.1(b)) and at longer times (not shown) it again becomes distant from the real axis. As we demonstrate below, the proximity of secondary branch (1) to the real axis directly affects the size of its contribution to the final wavefunction and therefore its role in interference effects. This proximity between the branches also coincides with the time when the caustic approaches

the real axis. Secondary branch (2) does not reach the vicinity of the real axis for any of the time scales in the figures below, hence its contribution to the final wavefunction (eq.(2.31)) is negligible (on the order of 10^{-35}). Consequently, from here on we ignore secondary branch (2) and refer to secondary branch (1) as *the* secondary branch.

As mentioned in sections II D-II E, the existence of more than one branch motivates the superposition of their contributions in the final wavefunction

$$\psi = \psi_{\rm R} + G\psi_{\rm S}; \quad \psi_{\rm R} = \exp\left(\frac{i}{\hbar}S_{\rm Real}\right),\ \psi_{\rm S} = \exp\left(\frac{i}{\hbar}S_{\rm Sec}\right), \tag{3.8}$$

where $S_{\rm Real}$ and $\psi_{\rm R}$ are the phase and wavefunction associated with the real branch, and $S_{\rm Sec}$ and $\psi_{\rm S}$ correspond to the secondary branch. G is Berry's smoothing function, eq.(2.33). In figs. 2(a-c) we compare the exact wavefunction with the numerical results obtained by applying CWKB. The figures indicate that when the wavefunction does not exhibit oscillations, for example at short times, the contribution of the real branch is sufficient to obtain a good approximation to the wavefunction and we can actually take $G = 0$ everywhere. At intermediate times, when the wavefunction exhibits interference effects, the contribution of both branches must be included.

The discussion in the previous paragraph suggests that there is a "crossover" phenomenon, i.e. that for certain values of x and t it is necessary to include both branches, and for others only one is needed (since the second contribution grows exponentially). This is the Stokes phenomenon described at section II E. The crossover phenomenon occurs in the vicinity of where a Stokes line crosses the real axis, X_C. In figs.3(a-c) we plot the contribution at $t_f = 5$, $t_f = 5.48$ and $t_f = 6$ of each individual branch and their superposition. In each case we see that for $x \gtrsim X_C$ there is a dramatic increase of ψ_S yielding a non-physical solution. Using Berry's smoothing function allows us to discard the non-physical solution in a smooth way. In fig.3(b) we also see another divergence where a caustic crosses the real axis (see appendix A).

It is interesting to examine in greater detail the contributions of the real and secondary branches to the final wavefunction and their dependence on t_f and x_f. The relative contribution of each branch is determined by the imaginary part of the phase since

$$|\psi_{\rm R}| = \left|\exp\left(\frac{i}{\hbar}S_{\rm Real}\right)\right| = \exp\left(-\frac{\Im(S_{\rm Real})}{\hbar}\right), \tag{3.9}$$

and similarly for $\psi_{\rm S}$ and $\Im(S_{\rm Sec})$. In figs.4(a) and 4(b) we plot $\Im(S_{\rm Real})$ and $\Im(S_{\rm Sec})$ respectively for a series of final times t_f. Clearly the secondary branch has a negligible contribution

at early and late times. This observation coincides well with the need to include the contribution of the secondary branch into the final wavefunction only at intermediate times. The growth of $\psi_{\rm S}$ seen in fig.3 is a direct consequence of the small negative value of $\Im(S_{\rm Sec})$ for $t_f = 5$, $t_f = 5.48$ and $t_f = 6$ seen in fig.4(b). The divergence caused by the caustic at $t_f = 5.48$ is seen very clearly in figs.4(a-b).

B. Second Order approximation, $N = 2$

We now examine the effect of incorporating S_2 in the CWKB approximation. In addition to the five equations needed to obtain the complex trajectories, S_0 and S_1, we need to solve eqs.(2.22)-(2.26). In fig.5(a) we depict the approximate wavefunction for $N = 2$ at $t_f = 6$. The $N = 2$ result (dashed line) yields a very good approximation to the exact result (solid line) and is better than the $N = 1$ result (fig.3(c)). For $x \gtrsim 23$, where only the real branch contribution is included, the improvement in the approximation over $N = 1$ is clearly visible. For $x \leq 22$ the improvement is less visible but still significant. In this region we calculated the relative error between the absolute value of the approximate and exact wavefunctions using all the data points depicted in figs.3 and 5(a). The results are presented in fig.5(b). For $N = 1$ the mean relative error is 0.34% while for $N = 2$ the mean relative error is 0.11%.

IV. SUMMARY

We have presented a formulation of complex time-dependent WKB (CWKB) that allows the incorporation of interfering contributions to the wavefunction. The central idea in CWKB as presented by Boiron and Lombardi[15] is to include both the amplitude and the phase in the lowest order term of the conventional time-dependent WKB method. This substitution treats the phase and the amplitude on an equal footing in the limit $\hbar \to 0$.

We have incorporated into the CWKB method the possibility of contributions from multiple crossing trajectories. Boiron and Lombardi claim (section V in reference[15]) that the root search procedure they use "excludes de facto such double contributions". As we have demonstrated here, allowing for multiple contributions leads to the description of interference effects that are absent from the Boiron-Lombardi formulation of CWKB. In addition, we have shown how to derive higher orders terms of the approximation in a straightforward

manner by using the Lagrangian derivative. This process was applied to the derivation of the $N = 2$ term in the CWKB approximation and the results obtained were better than for $N = 1$. In this paper we used the equations of motion of the Stokes lines and caustics combined with Berry's smoothing formula to deal with the effect of the Stokes phenomenon.

The CWKB method has several benefits. The derivation of the CWKB equations of motion is straightforward and simple. The trajectory equations of motion remain classical for any order of truncation. This observation is a consequence of the fact that there is no feedback in the CWKB equations of motion. The CWKB method allows for tunneling, as opposed to the Herman-Kluk method for example. Even though we do not demonstrate this here, the $N = 1$ CWKB equations of motion are identical to the $N = 2$ BOMCA equations[33] where deep tunneling has been demonstrated[30]. However, the method is not without its difficulties. First, the trajectories that emerge, although they obey classical equations of motion, propagate in the complex plane (due to complex initial conditions), requiring analytic continuation of the quantum wavefunction. A second drawback is that the reconstruction of the wavefunction on the real axis requires a root search process. This process can be eased by exploiting the analytic mapping between initial and final position. A third drawback is the appearance of caustics and Stokes lines that affect the accuracy of the formulation. Since WKB plays such a central role in quantum mechanics in general and in semiclassical mechanics in particular, we believe that the developments described in this paper could help make the time-dependent WKB formulation a competitive alternative to current time-dependent semiclassical methods.

We wish to acknowledge David Kessler and Uzi Smilansky for useful discussions. This work was supported by the Israel Science Foundation (576/04).

APPENDIX A: CAUSTIC DYNAMICS

In this appendix we sketch the derivation of how to trace the caustic as a function of time. A full derivation will appear in ref.[44]. The interest in the caustic position originates from the fact that Stokes lines emanate from it and complex semiclassical approximations break down in the caustic's vicinity. Suppose we have found a trajectory $x(t)$ and consider f and

g satisfying

$$\frac{d}{dt}\begin{pmatrix} g \\ f \end{pmatrix} = \begin{pmatrix} 0 & 1/m \\ -\partial_{xx}V(x(t)) & 0 \end{pmatrix}\begin{pmatrix} g \\ f \end{pmatrix}. \tag{A1}$$

Then

$$\frac{d}{dt}\left(\frac{f}{g}\right) = -\partial_{xx}V - \frac{1}{m}\left(\frac{f}{g}\right)^2. \tag{A2}$$

Equation (A2) is identical to eq.(2.21) if we identify $f/g = \partial_{xx}S_0$ and set the initial conditions in eq.(A1) to be $g(0) = 1$ and $f(0) = \partial_{xx}S_0(x,0)$. Since the equation of motion of S_1 (eq.(2.19)) involves $\partial_{xx}S_0$, S_1 diverges when $g = 0$. Thus, the divergence in S_1 can be traced by following the zero of g. To show that the zero of g corresponds to a caustic, note that g fulfils

$$\frac{d^2g}{dt^2} = -\frac{\partial_{xx}V}{m}g. \tag{A3}$$

Identifying

$$g(t) = \frac{\delta x(t)}{\delta x(0)}, \tag{A4}$$

where $\delta x(t)$ is the variation of the classical trajectory, we recognize eq.(A3) as the Jacobi equation — the equation of motion for the variation of Newton's second law. By definition, the caustic is located where the local spread of trajectories, $\delta x(t)$, is zero.

Suppose that we have found a trajectory, $x(t)$, for which at t_f we have $g(t_f) = 0$. Clearly, $X = x(t_f)$ is the position of a caustic. How will the caustic propagate as a function of time? We can write

$$\delta X = \delta(x(t_f)) = \delta x(t_f) + \frac{dx(t_f)}{dt}\delta t_f = g(t_f)\delta x(0) + \frac{dx(t_f)}{dt}\delta t_f = \frac{dx(t_f)}{dt}\delta t_f, \tag{A5}$$

hence

$$\frac{\delta X}{\delta t_f} = \frac{dx(t_f)}{dt}. \tag{A6}$$

We conclude that the velocity of the caustic equals the velocity of a trajectory that ends at the caustic. The RHS of eq.(A6) requires a supplementary equation of motion for the initial position that reaches the caustic at t_f. The derivation of such an equation of motion is a more cumbersome process and will appear in ref.[44]. Here we present the final result

$$\frac{\delta x(0)}{\delta t_f} = \frac{(f(t_f))^2}{m^2\partial_{xx}v(x(0)) - m\int_0^{t_f}\partial_{xxx}V(x(\tau))g^3(\tau)d\tau}, \tag{A7}$$

where $\partial_{xx}v(x(0))$ is the second spatial derivative of the initial velocity. For CWKB with an initial Gaussian wavepacket $\partial_{xx}v(x(0)) = \left.\frac{\partial_{xxx}S_0(x,0)}{m}\right|_{x=x_0} = 0$ (see eq.(3.4)). We emphasize

that eqs.(A6) and (A7) apply to any system that obeys classical dynamics. In fig.6 we plot the position of the caustic as a function of time. Notice that the position where the caustic crosses the real axis ($x \approx 23.5$, $t \approx 5.48$) can be identified with the spike seen in fig.3(b) and fig.4(a) at the same position.

Two final remarks: First, in section II D we mentioned that using the analyticity of the mapping $x(0) \mapsto x(t_f)$ is a key step in the root search process. The caustic is strongly related to the position where the inverse mapping has *branch points*. Defining the function $x_f(x_0)$ (where $x_f = x(t_f)$ and $x_0 = x(0)$), one sees that at the position where the spreading of trajectories is zero we have $\frac{\partial x_f}{\partial x_0} = 0$ and consequently $\frac{\partial x_0}{\partial x_f}$ is not defined. Second, it is well-known that time-dependent semiclassical approximations such as the van Vleck propagator diverge at caustics. Therefore, one may surmise that there is a close relationship between S_1 and the van Vleck determinant. This relationship will be developed more fully in ref.[44].

APPENDIX B: STOKES LINE DYNAMICS

In ref.[44] we give a full derivation of the equations of motion for the Stokes lines. In this appendix we present an overview of this derivation. CWKB can be viewed as an asymptotic expansion expressed as a sum of two exponentials, see eq.(2.34). The Stokes lines at time t can be defined as the locus of points x satisfing[17, 42]

$$\Re(S_0^1(x,t)) = \Re(S_0^2(x,t)), \tag{B1}$$

where $S_0^j(x,t)$, $j = 1, 2$, is the classical action associated with the two complex classical trajectories, $x_1 = x_1(\tau)$, $x_2 = x_2(\tau)$ that reach x at time t. For simplicity in this appendix we denote $S_j = S_0^j$. The variation of the action in relation to δt and δx is

$$\delta S_j(x,t) = \partial_t S_j(x,t)\delta t + \partial_x S_j(x,t)\delta x. \tag{B2}$$

Equation (B2) can be written as

$$\delta S_j(x,t) = -\left(\frac{1}{2}m\dot{x}_j^2 - V(x_j)\right)\delta t + m\dot{x}_j\delta x, \tag{B3}$$

by identifying $\partial_x S_j(x,t) = m\dot{x}_j$ and inserting $\partial_t S_j$ from eq.(2.9). Taking the variation of eq.(B1) and using eq.(B3) yields after a short manipulation

$$\Re\left(-\frac{1}{2}(\dot{x}_1^2 - \dot{x}_2^2)\delta t + (\dot{x}_1 - \dot{x}_2)\delta x\right) = 0. \tag{B4}$$

If we focus on the variation at a fixed time ($\delta t = 0$) we deduce from eq.(B4) that up to rescaling by a real factor

$$\delta x = i(\dot{x}_1 - \dot{x}_2). \tag{B5}$$

This allows us to follow the Stokes lines at a fixed time. The induced motion of the starting points of the two trajectories is given by relation (A4), $\delta x_j(0) = \frac{\delta x(t)}{g_j(t)}$. Note that the implementation of eq.(B5) requires an initial position on the Stokes line from which to start following the line. In fig.7 we plot two Stokes lines emanating from a caustic at $t = 5$. Notice the point at which the Stokes line crosses the real axis, X_C. The vicinity of X_C is where we apply Berry's smoothing formula, eq.(2.33).

Allowing for the variation of time we can write eq.(B4) as

$$-\frac{1}{2}(\dot{x}_1^2 - \dot{x}_2^2)\delta t + (\dot{x}_1 - \dot{x}_2)\delta x = i\lambda\delta t, \tag{B6}$$

where λ is an arbitrary real number. From eq.(B6) follows

$$\frac{\delta x}{\delta t} = \frac{i\lambda + \frac{1}{2}(\dot{x}_1^2(t) - \dot{x}_2^2(t))}{\dot{x}_1(t) - \dot{x}_2(t)}. \tag{B7}$$

The arbitrariness of λ corresponds to the fact that when looking at the motion of a point on a curve the point can freely move in the tangent direction to the curve without changing the overall curve motion. Equation (B7) allows us to follow X_C as it is varied. Suppose that at some initial time we know the crossing point. We can now choose λ in such a way that the LHS of eq.(B7) stays real, hence obtaining an equation of motion for X_C — eq.(2.35) (see ref.[44]). We can also show that the induced motion of the starting points of the two trajectories is given by

$$\frac{\delta x_j(0)}{\delta t} = \frac{1}{g_j(t)}\left(\frac{\delta x_j}{\delta t} - \dot{x}_j(t)\right). \tag{B8}$$

In fig.8 we plot X_C as a function of time and zoom in on the time when the caustic crosses the real axis. There is a numerical problem at this time because the denominator of (B7) vanishes at the caustic.

---

[1] G. Wentzel, Z. Phys. **38**, 518 (1926); H. A. Kramers, Z. Phys. **39**, 828 (1926) ;L. Brillouin, CR Acad. Sci, Paris **183**, 24 (1926); L. Brillouin, J. Phys., **7**, 353 (1926)

[2] W. Pauli, *Die allgemeine Prinzipien der Wellenmechanik*, in *Handbuch der Physik*, H. Geiger and K. Scheel, eds., Vol 24, Part 1, 2nd ed., Springer-Verlag, Berlin, 1933, pp. 83-272.

[3] K. Gottfried, *Quantum Mechanics, Volume I: Foundations* (W. A. Benjamin, New York, 1966).

[4] Byung Chan Eu, W. J. Chem. Phys. **57**, 2531 (1972).

[5] H. J. Korsch, R. Mohlenkamp, Phys. Lett. A **67**, 110 (1978).

[6] S. M. Blinder, Chem. Phys. Lett. **137**, 288 (1987).

[7] L. Raifeartaigh, A. Wipf, Found. Phys. Lett. **18**, 307 (1987).

[8] M. P. A. Fisher, Phys. Rev. B **37**, 75 (1988).

[9] R. Rubin, Junior paper (Princeton, 1990).

[10] M. Burdick, H. J. Schmidt, J. Phys. A: Math. Gen. **27**, 579 (1994).

[11] C. Sparber, P. A. Markowich, N. J. Mauser, arXiv:math-ph/0109029 (2002).

[12] A. S. Sanz, F. Borondo, S. Miret-Artés, J. Phys.:Condens. Matter **14**, 6109 (2002).

[13] Jeong Ryeol Choi, Int. J. Theo. Phys. **43**, 947 (2004).

[14] P. Bracken, arXiv:math-ph/0608011v2 (2006).

[15] M. Boiron, M. Lombardi, J. Chem. Phys. **108**, 3431 (1998).

[16] D. Huber, E. Heller, J. Chem. Phys. **87**, 5302 (1987).

[17] D. Huber, E. Heller, R. G. Littlejohn, J. Chem. Phys. **89**, 2003 (1988).

[18] M. Baranger, M. A. M.de Aguiar, F. Keck, H. J. Korsch, B. Schellhaa, J. Phys. A: Math.Gen. **34**, 7227 (2001).

[19] M. A. M. de Aguiar, M. Baranger, L. Jaubert, F. Parisio, A. D. Ribiero, J. Phys. A: Math.Gen. **38**, 4645 (2005).

[20] F. Parisio, M. A. M. de Aguiar, J. Phys. A: Math.Gen. **38**, 9317 (2005).

[21] M. A. M. de Aguiar, M. Baranger, L. Jaubert, F. Parisio, A. D. Ribeiro, J. Phys. A **38**, 4645 (2005).

[22] A. D. Ribeiro, M. Novaes, M. A. M. Aguiar, Phys. Rev. Lett. **95** 050405 (2005).

[23] A. D. Ribiero, M. A. M. de Aguiar, M. Baranger, Phys. Rev. E **69**, 066204 (2004).

[24] M. Novaes, M. A. M.de Aguiar, Phys. Rev. A **72**, 032105 (2005).

[25] A. D. Ribiero, M. A. M. de Aguiar, arXiv:0704.2510v1 [quant-ph] (2007).

[26] J. L. Klauder, in "Random media" (G. Papanicolauou, ed.), IMA Series in Mathematics and its applications **7**, Springer-Verlag, New-York, 163 (1987).

[27] Y. Weissman, J. Chem. Phys. **76**, 4067 (1982); J. Phys. A **16**, 2593 (1983).

[28] S. Adachi, Ann. Phys. **195**, 45 (1989).

[29] A. Rubin, J. L. Klauder, Ann. Phys. **241**, 212 (1995).

[30] Y. Goldfarb, I. Degani, D. J. Tannor, J. Chem. Phys. **125**, 231103 (2006).

[31] Y. Goldfarb, D. J. Tannor, J. Chem. Phys. **127**, 161101 (2007).

[32] Y. Goldfarb, J. Schiff, D. J. Tannor, J. Phys. Chem. A **111**, 10416 (2007).

[33] Y. Goldfarb, *Solution of the Time-Dependent Schrödinger Equation via Complex Quantum Trajectories*, Ph.D diss., Weizmann Institute of Science (2007).

[34] B. A. Rowland, R. E. Wyatt, J. Phys. Chem. A **111**, 10234 (2007).

[35] Chia-Chun Chou, R. E. Wyatt, Phys. Rev. A **76**, 012115 (2007).

[36] M. V. Berry, K. E. Mount, Rep. Prog. Phys. **35**, 315 (1972).

[37] M. C. Gutzwiller, *Chaos in Classical and Quantum Mechanics* (Springer-Verlag, New York, 1990).

[38] G. G. Stokes, Trans. Camb. Phil. Soc. **10**, 106 (1864).

[39] A. Shudo, K. S. Ikeda, Phys. Rev. Lett. **74**, 682 (1995); Phys. Rev. Lett. **76**, 4151 (1996).

[40] R. G. Littlejohn, Phys Rev. Lett. **54**, 1742 (1985).

[41] N. T. Maitra, E. J. Heller, Phys. Rev. A **61**, 012107 (1999).

[42] M. V. Berry, Proc. R. London, Ser. A **422**, 7 (1989).

[43] T. Van Voorhis, E. J. Heller, J. Chem. Phys. **119**, 12158 (2003).

[44] J. Schiff, Y. Goldfarb, D. J. Tannor, in preparation.

[45] N. Bleistein, R. A. Handelsman, *Asymptotic Expansion of Integrals* (Dover Publications, New York, 1986).

[46] T. Shnerb, K. G. Kay, Phys. Rev. E **73**, 046202 (2006).

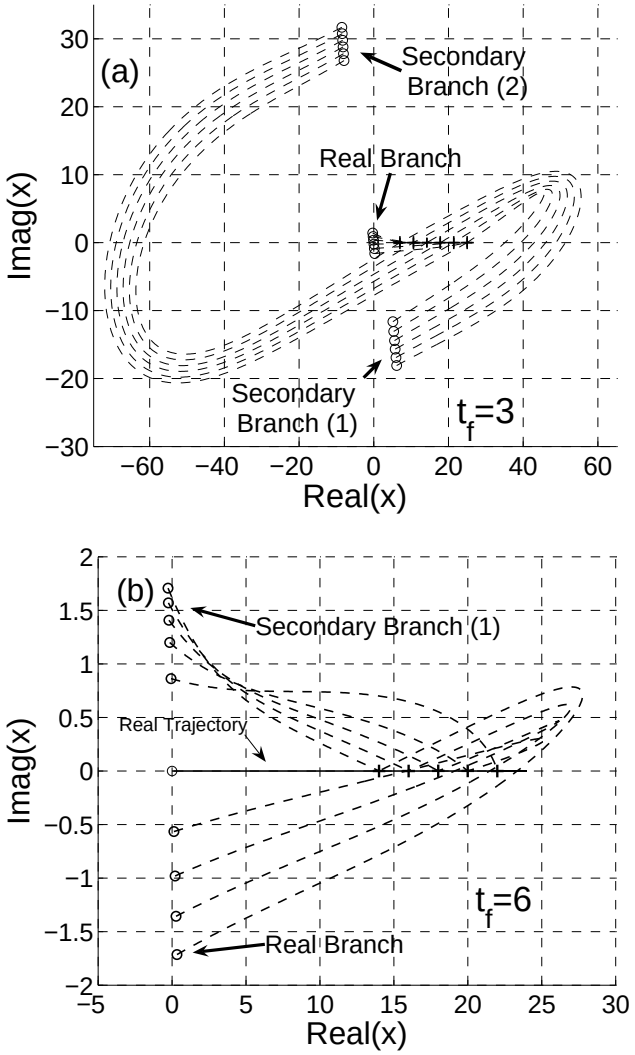

FIG. 1: Complex classical trajectories with initial positions (marked as circles) and *real* final positions (marked as pluses) at (a) $t_f = 3$ and (b) $t_f = 6$. The trajectories arise from an initial Gaussian wavepacket propagating in a quartic double-well potential. The Gaussian is centered at $x = 0$ and has positive initial momentum (the parameters are given in the text). In plot (a), each final position arises from three initial positions whereas in plot (b) although there are also three contributions to each final position, secondary branch (2) is quite distant and not shown in the plot. The initial positions are divided into a real branch and two secondary branches. The real branch is defined as incorporating a trajectory that remains on the real axis at all times. The real trajectory is specifically indicated in plot (b).

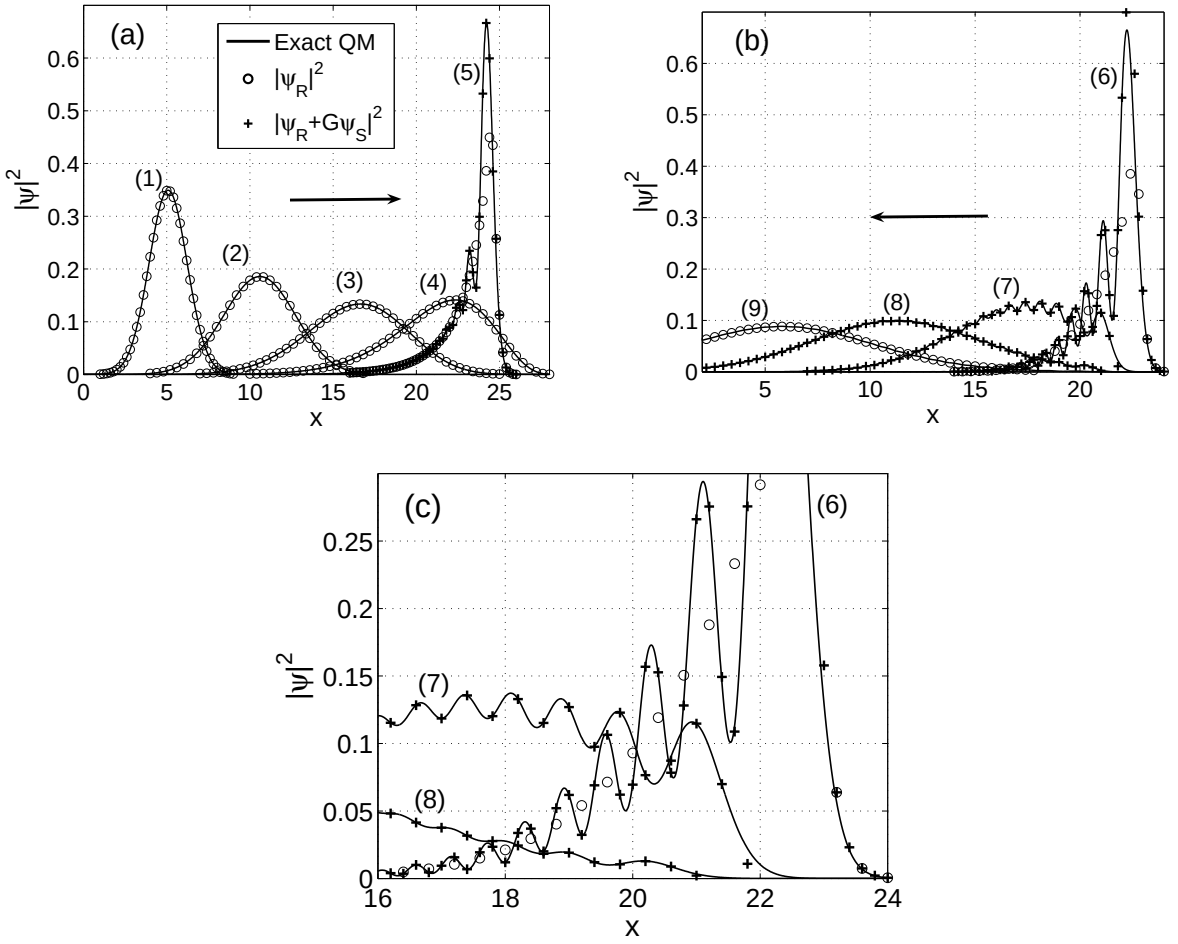

FIG. 2: A comparison between the exact quantum wavefunction and CWKB ($N = 1$), using a two-branch superposition and Berry's smoothing formula (eq.(2.33)). X_C needed for Berry's formula was calculated using the equation of motion (2.35). The comparison is at a series of final times t_f specified by the numbers in the parentheses. The plots arise from an initial Gaussian wavepacket centered at $x = 0$ with a positive average momentum, propagating in a quartic double-well potential (the parameters are given in the text). (a) Initially right-propagating wavefunction; (b) the reflected wavefunction; (c) a zoom on a section of (b). For $t_f = 5$ in (a) and $t_f = 6$ in (b) and (c) we plot the results both for just the real branch $|\psi_{\rm R}|^2$ and for the superposition of branches $|\psi_{\rm R} + G\psi_{\rm S}|^2$. The interference pattern obtained by superposing $\psi_{\rm R}$ and $\psi_{\rm S}$ is clearly observed.

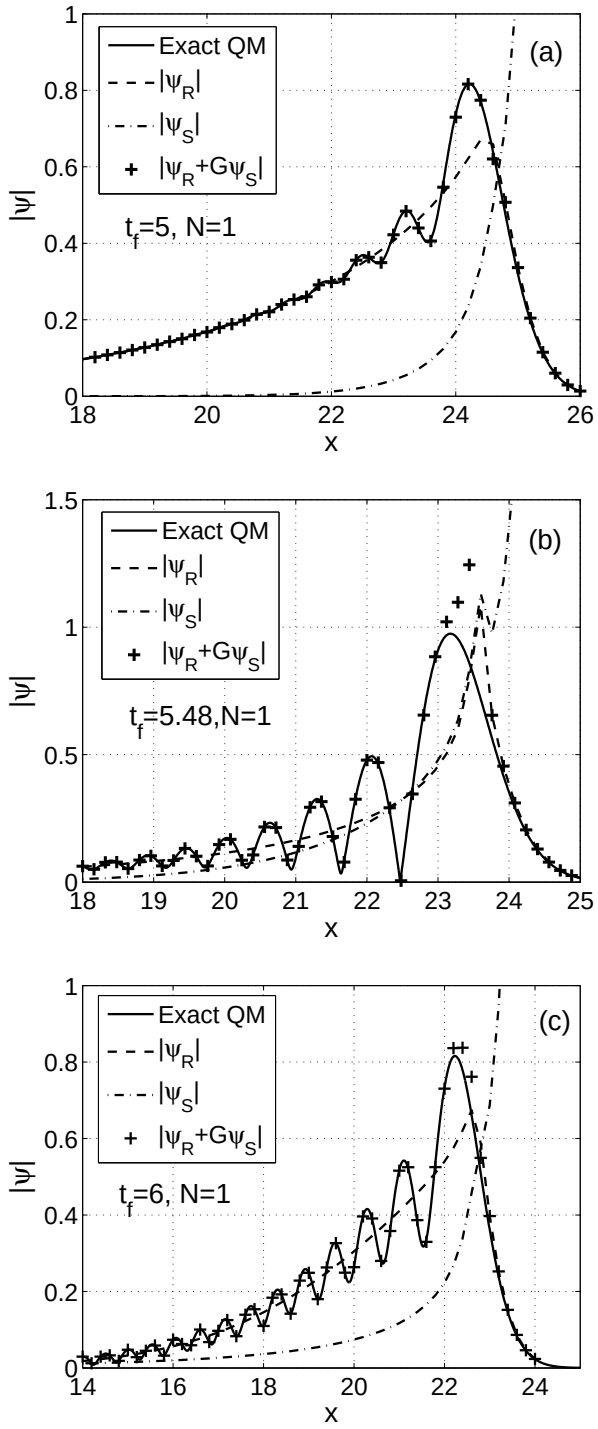

FIG. 3: A close examination of the CWKB approximation at (a) $t_f = 5$, (b) $t_f = 5.48$ and (c) $t = 6$ for $N = 1$. The contributions of each branch to the wavefunction are depicted by plotting $|\psi_{\rm R}|$, $|\psi_{\rm S}|$ and $|\psi_{\rm R} + G\psi_{\rm S}|$. Note the dramatic increase of $\psi_{\rm S}$ for $x \gtrsim X_C$. X_C equals roughly 24.5, 23.5, 22,6 when t_f equals 5, 5.48 and 6, respectively. Note that $t_f = 5.48$ is when the caustic crosses the real axis.

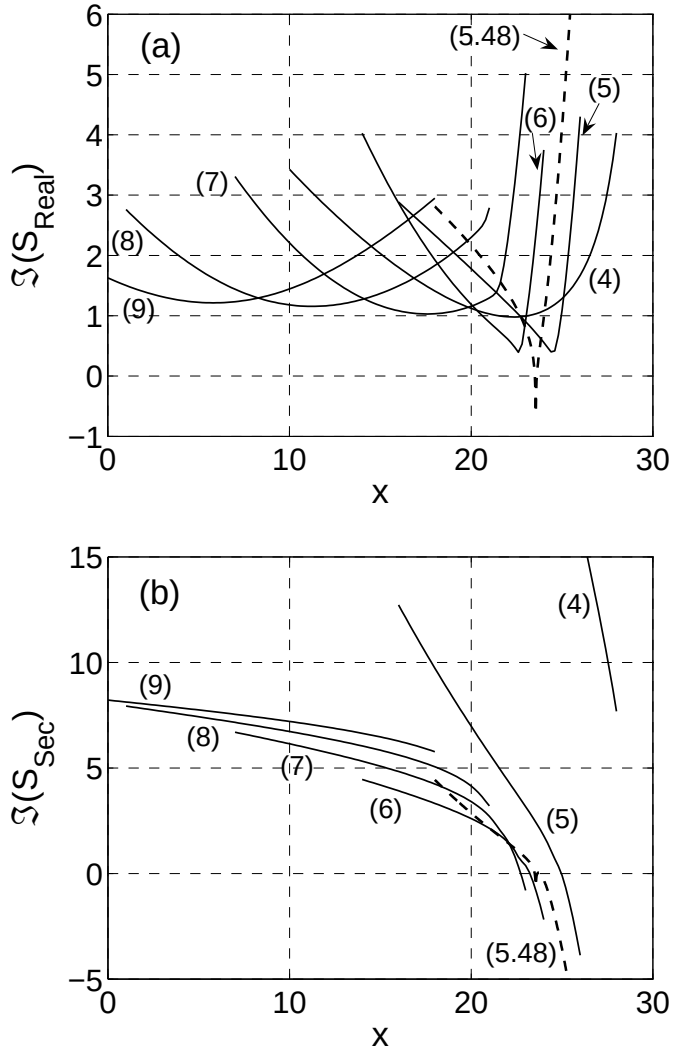

FIG. 4: (a) $\Im(S_{\rm Real})$ and (b) $\Im(S_{\rm Sec})$ are depicted at a series of final times t_f (given in the parentheses, where the dashed lines are for $t_f = 5.48$). The results are limited to the spatial interval for which the absolute value of the exact wavefunction is significantly larger than zero. The imaginary part of the phase allows for a qualitative estimate of the contribution of each branch to the probability $|\psi_{\rm R} + G\psi_{\rm S}|^2$ (see eq.(3.9)). Figure 4(b) shows that $\Im(S_{\rm Sec})$ drops below ~ 2 only for a finite interval of intermediate times. Therefore, only for this range of times does the secondary branch makes a significant contribution to the wavefunction. The divergence caused by the caustic as it crosses the real axis at $t_f = 5.48$ is clearly evident in plot (a) (it may be seen in plot (b) as well although less clearly).

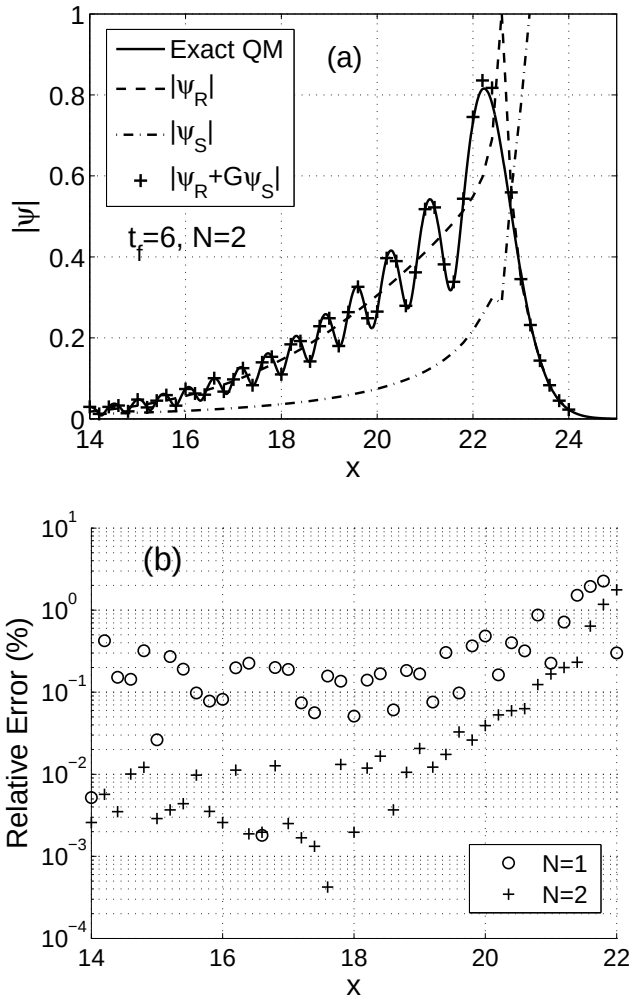

FIG. 5: (a) The second order ($N = 2$) CWKB approximation is depicted for $t_f = 6$. A discontinuity appears at $X_C \simeq 22.6$ for both $\psi_{\rm R}$ and $\psi_{\rm S}$. (b) The relative error between the absolute value of the exact quantum wavefunction and the CWKB approximation for $N = 1$ and $N = 2$, based on the data in fig.3(c) and fig.5(a). A comparison of the relative errors indicates a clear improvement when taking an additional order in the CWKB approximation.

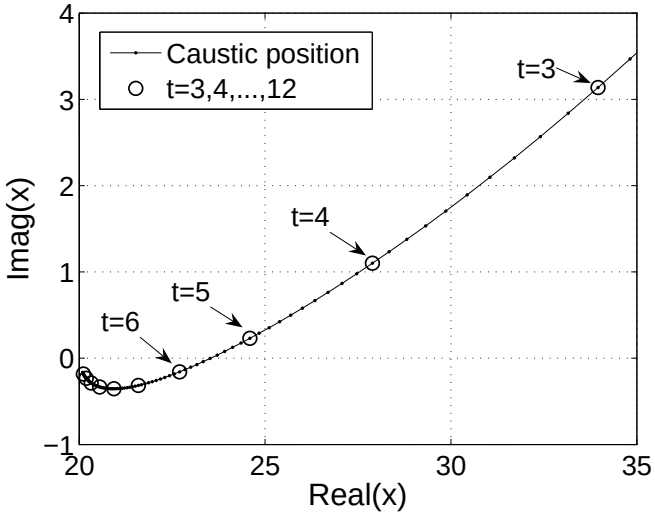

FIG. 6: Caustic position as a function of time, calculated by following the divergence of S_1 (see appendix A, eqs.(A6)-(A7)). The effect of the caustic crossing the real axis at $t_f \approx 5.48$ can be clearly seen in the spikes in figs. 3(b) and 4(a).

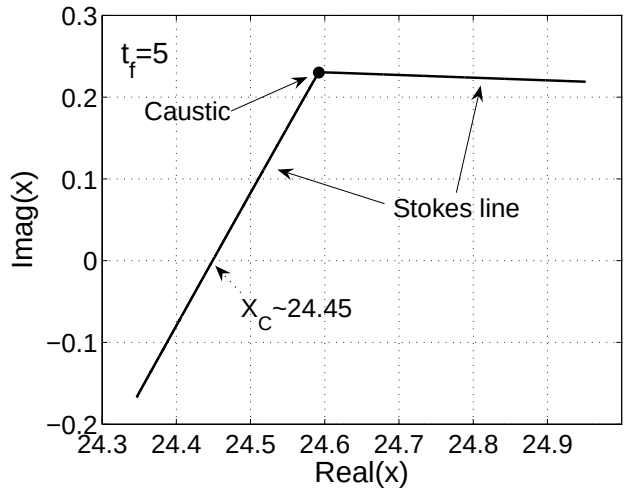

FIG. 7: Stokes lines at time $t_f = 5$. The calculation of these plots required finding a single position that fulfils condition (B1) and then using eq.(B5) to trace the Stokes lines. The position where the Stokes line crosses the real axis is depicted explicitly.

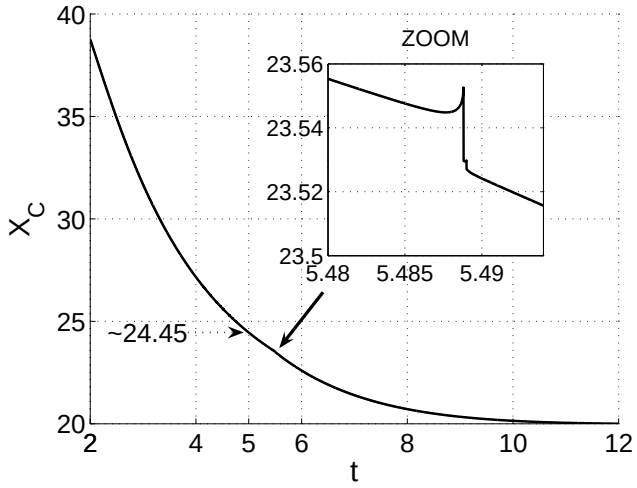

FIG. 8: The position where a Stokes line crosses the real axis, X_C, is depicted as a function of time. This position is needed for the use of Berry's smoothing formula (eq.(2.33)). This plot was obtained by finding X_C at some initial time and then using eq.(B7) to propagate it. We see that at $t \simeq 5.48$, when the caustic crosses the real axis, there is a spike in X_C. This comes about since the Stokes lines emanate from the caustic, and thus when the caustic crosses the real axis the denominator in eq.(B7) vanishes.